8. A. Engel, Ionized Gases [Russian translation], Moscow (1959).
9. Yu. P. Raizer, Principles of the Modern Physics of Gas Discharge Processes [in Russian], Moscow (1980).

THERMAL DESTRUCTION OF SPHERICAL ICE PARTICLES UNDER THE ACTION OF RADIATION WITH λ = 10.6 μm

A. P. Prishivalko, L. P. Semenov, L. G. Astef'eva, and S. T. Leiko

UDC 551.511;517.944

Questions involving interaction of laser radiation with material in the dispersed state (ice particle destruction) are considered.

As was shown in [1], action of intense radiation at a wavelength of 10.6 μm on lamellar ice crystals produces inhomogeneous temperature fields which lead to the appearance of elastic stress fields. For high inhomogeneity of the temperature field the temperature changes within the crystals can reach values such that tensile elastic stresses become greater than the failure stress for ice, equal to $2 \cdot 10^6$ N/m^2. In this case failure (cracking) of the crystal occurs with formation of smaller ice particles.

In the subcloud layer of crystalline or mixed clouds small ice particles of spherical or almost spherical form may exist. Like lamellar crystals, spherical ice particles can be destroyed by the action of intense radiation at λ = 10.6 μm due to inhomogeneous internal heat liberation, while not reaching the melting temperature. The present study will attempt to evaluate conditions and energy expenditures for thermal destruction of spherical ice particles under radiant action.

In the general case the ice particles have a hexagonal crystalline lattice with a weakly expressed anisotropy in both optical and elastic properties. However, real crystals formed in the atmosphere contain microimpurities, have large numbers of point defects and other structural faults, which under the conditions of the problem being considered allow us to consider the crystal as being isotropic. The heat liberation Q at a specified point within a homogeneous spherical particle with coordinates r, θ, ϕ is defined by the expression [2]

$$Q = \frac{4\pi n \varkappa}{m_m \lambda} IB, \tag{1}$$

where $B = (E, E_r^* + E_\theta E_\theta^* + E_\phi E_\phi^*) E_0^{-2}$. At λ = 10.6 μm for ice n = 1.097, κ = 0.134.

From the behavior of the curves of Fig. 1 it is evident that as in a water droplet [2], heat liberation within the ice particle volume is inhomogeneous, especially in particles with a radius $R \gg 10$ μm. In contrast to water droplets, here we find no large maxima in heat liberation near the dark surface of the particle. The major heat liberation occurs on the illuminated surface. This is explained by the fact that the real component of the index of refraction of ice is somewhat lower than that of water, while the imaginary component is significantly higher [3].

The problem of destruction of an ice crystal suspended in air under the action of thermoelastic stresses initiated by intense laser radiation reduces to simultaneous solution of the equilibrium [4] and thermal conductivity equations

$$\frac{3(1-\sigma)}{1+\sigma} \nabla \operatorname{div} \mathbf{u} - \frac{3(1-2\sigma)}{2(1+\sigma)} \operatorname{rot} \operatorname{rot} \mathbf{u} = \gamma \nabla T, \tag{2}$$

$$c\rho \frac{\partial T}{\partial t} = \lambda_1 \Delta T + Q(r, \theta, \varphi, n, \varkappa, \lambda, t, I) \tag{2a}$$

with appropriate boundary and initial conditions.

Physics Institute, Academy of Sciences of the Belorussian SSR, Minsk. Translated from Inzhenerno-Fizicheskii Zhurnal, Vol. 54, No. 1, pp. 103-108, January, 1988. Original article submitted October 16, 1986.

 0022-0841/88/5401-0080 $ 12.50

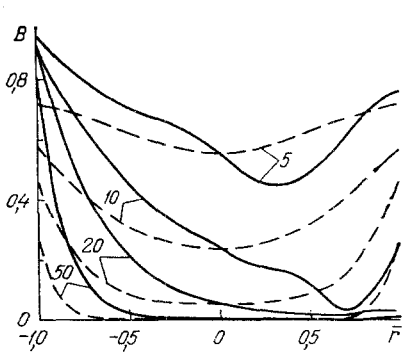

Fig. 1

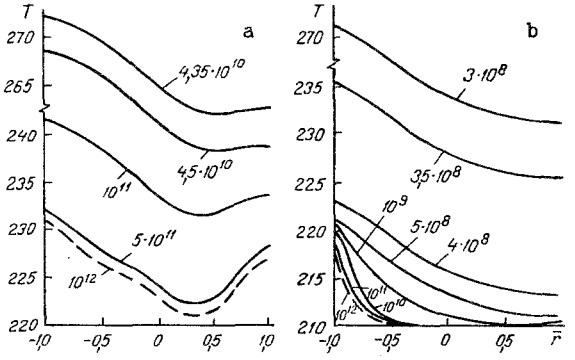

Fig. 2

Fig. 1. Distribution of dimensionless absorbed energy in particle section along diameter coinciding with direction of radiation (solid curves) and along direction perpendicular to radiation (dashes). Digits along curves are R values, μm. Radiation propagates from left to right.

Fig. 2. Distribution of temperature T, K, along major diameter of particle with radius R = 5 (a) and 50 μm (b) before commencement of failure (radiation intensity I, $W \cdot m^{-2}$, indicated on curves). Radiation propagates left to right.

In the general case the radiation field distribution within the volume of the spherical particle is inhomogeneous [2]. This fact significantly complicates solution of the problem.

In principle, it is possible to obtain an approximate solution if we divide the problem into two parts. In the first stage we use Eq. (2) to determine the value of heating at which the appearance of cracks in the crystal is possible, and in the second stage, knowing the critical heating, by solution of the thermal conductivity problem we find the intensity of the radiation at which such heating occurs.

For crystals sufficiently small compared to the wavelength it is simplest to evaluate the critical heating by commencing from the solution of the spherically symmetrical problem of deformation of a nonuniformly heated sphere with a temperature maximum at its center. The solution of this problem is well known [4] and leads to the following expression for the highest tensile stress $\sigma_{\theta\theta}$ in the crystal:

$$\sigma_{\theta\theta} = 2\mu\gamma \frac{1+\sigma}{1-\sigma} \frac{1}{R^3} \int_0^R T(r) r^2 dr. \tag{3}$$

For our evaluation we assume that the temperature distribution within the particle is characterized approximately by the expression

$$T = \Delta_1 T \left[1 - \left(\frac{r}{R} \right)^n \right], \tag{4}$$

where $1 \leqslant n \leqslant 2$.

Taking the value of the tensile stress equal to the failure point for ice $2 \cdot 10^6$ N/m^2 and using values typical of ice crystals $\sigma = 0.3$; $\gamma = 1.5 \cdot 10^{-4}$ K^{-1}, $\mu = 4 \cdot 10^9$ $N \cdot m^{-2}$, we obtain an estimate of the heating which leads to cracking of an ice sphere ΔT = 7-10 K. This estimate was obtained for small spherical crystals of pure ice. For real crystals with the dimensions considered in the present study (R = 5-50 μm), we will take the upper limit ΔT = 10 K.

To solve the problem we will use the algorithm and solution method for the two-dimensional thermal conductivity problem described in detail in [2]. In doing this we will eliminate from consideration situations in which the phase transition point T = 273 K is reached before conditions for fracture of the ice (lower radiation intensities, slow heating). Elimination of the phase transition permits use of the boundary condition

$$-\lambda_1(T) \left. \frac{\partial T}{\partial r} \right|_{r=R} = \alpha [T(R, \theta, t) - T_m,]. \tag{5}$$

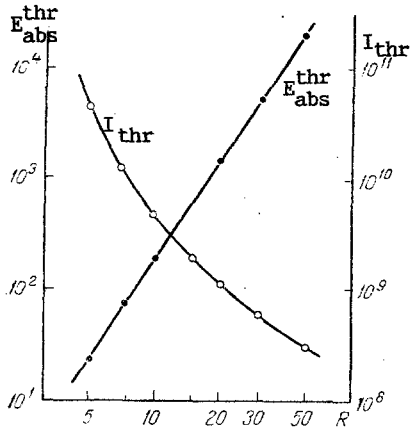

Fig. 3

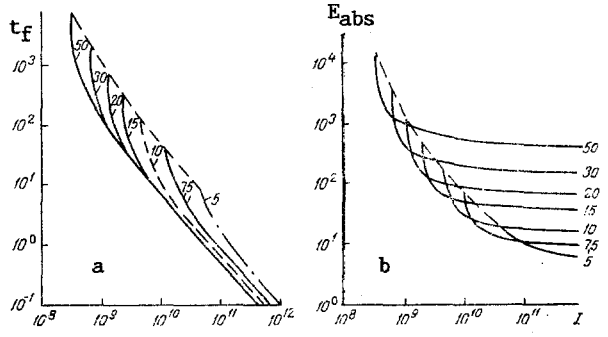

Fig. 4

Fig. 3. Threshold radiation intensity and threshold energy absorbed before failure vs particle radius. I_{thr}, $W \cdot m^{-2}$; E^{thr}_{abs}, μJ; R, μm.

Fig. 4. Time from commencement of laser action to particle failure (a) and energy absorbed (b) vs radiant intensity for particles of various radii (shown on curves). t_f, μsec; E_{abs}, μJ.

As usual [2], we use a locally one-dimensional implicit scheme, which we solve by the drive method. Since the range of temperature change within the particle in the present study is not large (from 210 to 273 K), density changes due to ice temperature change were not considered ($\rho = 0.092$ g·cm^{-3}). Variable values of $\lambda_1(T)$ and $c(T)$ were introduced in accordance with temperature values at each node of the grid at each time step using approximating expressions constructed from data of [5, 6] and having the form:

$$\lambda_1 = 615{,}46T^{-1}\ W \cdot m^{-1} \cdot K^{-1}, \tag{6}$$

$$c = (7{,}272T + 1101{,}128)\ J \cdot kg^{-1} \cdot K^{-1}. \tag{7}$$

The error in the approximation of tabular λ_1 and c values with Eqs. (6), (7) does not exceed 18-20 and 2%, respectively.

The calculation conditions allowed achievement of an uncertainty in the temperature values of no more than 20%. The step in radius was chosen as a function of particle radius: for R = 5-9 μm N = 25, for R = 10-25 μm N = 50, and for R $\geq$ 30 μm N = 100. In all cases the step-in angle was equal to 5°. The time step was determined by particle radius and the intensity of the acting radiation. For rapid regimes (high intensity) 150-300 time steps are sufficient. For intensities close to the threshold value (see below), the system is more critical with respect to choice of the time step (slow heating). In these situations the number of time steps is of the order of 2000-3000.

The heat exchange coefficient α on the particle surface is not large and does not play a significant role in the present problem. Variation in this quantity over four orders of magnitude led to temperature changes not exceeding tenths of a degree.

As has already been noted, in the present study we consider only such incident radiation intensity at which the temperature difference of $\Delta T = 10$ K within the particle is achieved before melting can commence at any point (T = 273 K). The lowest intensity value for which this condition is still fulfilled for particles of a given size will be termed the threshold intensity for thermal destruction of the ice particle.

This regime of ice particle heating differs significantly from heating of a water particle by intense radiation. Because the surface of a water droplet can cool more intensely by transforming a portion of its mass to the vapor state, the temperature distribution along the major diameter of the droplet is characterized by two temperature maxima, located near the illuminated and dark surfaces of the droplet.

Since in the present study we do not consider phase transitions, and heat exchange with the surrounding medium is small, the temperature maximum is localized directly on the illuminated surface of the ice particle (Fig. 2).

The position of the temperature minimum depends on the particle size and radiation intensity. As a result the maximum temperature differential occurs between some finite region on the illuminated portion of the surface and close thereto and a) a region of finite size located in the dark hemisphere (small particles, high intensity); b) a region of finite size located on the dark surface and close thereto (the most typical case for the particle sizes and intensities considered here); c) a large region encompassing practically all the dark hemisphere (large particles, high intensities). The distance between the maximally and minimally heated regions comprises from 0.5R to (1.7-1.9)R.

As is evident from Fig. 3, the threshold radiation intensity decreases rapidly with increase in particle size, while the amount of energy expended to failure increases. The corresponding functions can be represented by approximate expressions of the form

$$\lg I_{thr} = 5{,}66\,(\lg R)^{-0{,}445} - 4, \tag{8}$$

$$E_{abs}^{thr} = 0{,}174R^3 = 0{,}0415v \tag{9}$$

(v, μ^3). the error of Eqs. (8), (9) does not exceed ± 10%.

For particles with $R \geq 20$ μm at $I \geq 5 \cdot 10^9$ W·m^{-2} there is an inverse power dependence of time from the commencement of particle irradiation to failure as a function of incident intensity (see Fig. 4a). For particles with R = 15 μm such a dependence sets in at $I \geq 10^{10}$ W·m^2, for R = 10 μm, at $I \geq 10^{11}$ W·m^{-2}, and for $R \approx 5$ μm, at $I \geq 2 \cdot 10^{11}$ W·m^{-2}.

Two segments can clearly be distinguished in the curves of Fig. 4b. One is near the threshold intensity values with a very intense dependence of absorbed energy upon U. The second has a quite weak I dependence at high radiation intensities. In this interval for each R value the functions $E_{abs}(I)$ tend to some asymptotic value E_{abs}. While at threshold intensities of the incident radiation the energy expenditures for fracture of the particle are proportional to particle volume (see Eq. (9)), at high intensities the asymptotic value of this expenditure is proportional to particle cross section. It is evident from Fig. 4b that for particles with R > 7 μm with an error of not more than 10% the approximate relationship

$$E_{abs} = 0{,}166R^2 = 0{,}053S, \tag{10}$$

is valid, where S is measured in μm^2.

The relationships derived and conclusions reached here are valid over the indicated range of particle sizes for radiation intensities exceeding threshold values. since the presence of impurities usually changes the real component of the complex index of refraction only insignificantly, but can significantly increase the imaginary component, the failure criteria chosen herein are most probably elevated. This may affect to some degree the quantitative, but not the qualitative nature of the physical picture of the phenomena in question.

NOTATION

λ, radiation wavelength; Q, quantity of heat liberated per unit time per unit volume of material; r, θ, φ, spherical coordinates of point; m_m, index of refraction of medium surrounding particle; I, intensity of incident radiation; n and κ, real and imaginary components of complex index of refraction of particle material; E_0, electric field intensity in incident wave; E_r, E_θ, E_ϕ, electrical field components at given point within particle; **u**, deformation vector; σ, Poisson coefficient; T, temperature; γ, volume coefficient of expansion of ice; ρ, c, λ_1, specific density, heat capacity, and thermal conductivity; μ, shear modulus; R, radius of sphere being heated; $\Delta_1 T$, heating of sphere center relative to surface; α, heat exchange coefficient for particle material with surrounding medium; T_m, temperature of medium; v, particle volume; E_{abs}, energy expended in particle fracture; S, particle cross section.

LITERATURE CITED

1. P. N. Svirkunov and L. P. Semenov, Atmospheric Optics, Proceedings of the Experimental Meteorology Institute, No. 11 (54) [in Russian], Moscow (1975), pp. 3-18.
2. A. P. Prishivalko, Optical and Thermal Fields within Light-Scattering Particles [in Russian], Minsk (1983).

3. T. W. Schaff and D. Williams, J. Opt. Soc. Am., 63, No. 6, 726-732 (1973).
4. L. D. Landau and E. M. Lifshits, Mechanics of Continuous Media [in Russian], Moscow (1954).
5. A. Misnar, Thermal Conductivity of Solids, Liquids, Gases, and Their Composites [in Russian], Moscow (1968).
6. L. V. Gurvich, I. V. Veits, V. A. Medvedev, et al., Thermodynamic Properties of Individual Materials [in Russian], Vol. 1, Book 2, Moscow (1978).

RADIATIVE PARAMETERS OF SUSPENDED SULFIDE-CHARGE PARTICLES

M. N. Abramzon, F. N. Lisin, and L. N. Podobedova

UDC 536.3.621.745.32

Electromagnetic theory has been used to calculate the attenuation and scattering coefficients together with the spectral degree of blackness for polydisperse sulfide particles in a flame.

When high-intensity flame melting is applied to sulfides in nonferrous metallurgy, it is necessary to know the radiative parameters for the suspended-particle flows. Here we examine the radiation parameters for suspended particles of copper and lead–zinc charges.

Mie's theory [1] gives the radiation parameters for a single particle. Sulfide particles reacting with oxygen in a flame are covered by oxides; for example, a pyrrhotite particle may have a core composed of the initial material covered by layers of FeO, Fe_3O_4, and Fe_2O_3. One has to calculate the scattering properties for such a multilayer particle. From the viewpoint of electrodynamics, this is a boundary-value problem in diffraction for Maxwell's equations. Convenient formulas have been derived as recurrent relations between the Mie coefficients for particles having n and n + 1 layers:

$$a_l^{(n+1)} = \frac{y_{n+1}\psi_l(y_{n+1})\,p_l(Z_{n+1};a_l^{(n)}) - Z_{n+1}\psi_l'(y_{n+1})}{y_{n+1}\zeta(y_{n+1})\,p_l(Z_{n+1};a_l^{(n)}) - Z_{n+1}\zeta_l'(y_{n+1})}, \tag{1}$$

$$b_l^{(n+1)} = \frac{Z_{n+1}\psi_l(y_{n+1})\,p_l(Z_{n+1};b_l^{n}) - y_{n+1}\psi_l'(y_{n+1})}{Z_{n+1}\zeta_l(y_{n+1})\,p_l(Z_{n+1};b_l^{n}) - y_{n+1}\zeta_l'(y_{n+1})}, \tag{2}$$

where

$$p_l(\chi;\ f) = \frac{\psi_l'(\chi) - f\zeta_l'(\chi)}{\psi_l(\chi) - f\zeta_l(\chi)};\quad Z_n = K_n r_n;\quad y_n = K_{n+1} r_n;\quad K_i = \frac{2\pi}{\lambda} m_i;$$

$$\psi_l(\chi) = \sqrt{\frac{\pi\chi}{2}}\, J_{l+1/2}(\chi);$$

ζ_ℓ, a Riccati–Bessel function; r_n, radius of layer n; m, complex refractive index; and λ, wavelength.

The attenuation and scattering coefficients for such a particle are

$$k_{at\ \lambda} = \frac{2}{\rho^2}\sum_{l=1}^{\infty}\mathrm{Re}\{a_l + b_l\}, \tag{3}$$

$$k_{sc\ \lambda} = \frac{2}{\rho^2}\sum_{1}^{\infty}(2l+1)(|a_l|^2 + |b_l|^2), \tag{4}$$

where $\rho = 2\pi r_p \lambda$, r_p is particle radius.

The spectral attenuation and scattering coefficients averaged over the particle sizes and the mean scattering cosine for phase i are

All-Union Nonferrous Metal Processing Power Consumption Research Institute, Sverdlovsk.
Translated from Inzhenerno-Fizicheskii Zhurnal, Vol. 54, No. 1, pp. 108-111, January, 1988. Original article submitted September 9, 1986.

 0022-0841/88/5401-0084 $12.50